frontiers | Frontiers in Astronomy and Space Sciences

TYPE Original Research
PUBLISHED 01 September 2023
DOI 10.3389/fspas.2023.1251743

OPEN ACCESS

EDITED BY
Denise Piatti,
University of Padua, Italy

REVIEWED BY
Andres Arazi,
National Atomic Energy Commission, Argentina
Giuseppe Ferdinando D'Agata,
University of Catania, Italy

*CORRESPONDENCE
S. B. Dubovichenko,
dubovichenko@gmail.com

RECEIVED 02 July 2023
ACCEPTED 10 August 2023
PUBLISHED 01 September 2023

CITATION
Dubovichenko SB, Yeleusheva BM, Burkova NA and Tkachenko AS (2023), The reaction rate of radiative n^8Li capture in the range from 0.01 to 10 T_9. *Front. Astron. Space Sci.* 10:1251743. doi: 10.3389/fspas.2023.1251743

The reaction rate of radiative n^8Li capture in the range from 0.01 to 10 T_9

S. B. Dubovichenko[1]*, B. M. Yeleusheva[1,2], N. A. Burkova[1,2] and A. S. Tkachenko[1]

[1]Fesenkov Astrophysical Institute, Almaty, Kazakhstan, [2]Department of Physics and Technology, Al-Farabi Kazakh National University, Almaty, Kazakhstan

Within the modified potential cluster model (MPCM) with forbidden states, the total cross sections are calculated for capture in the ground and first excited states of the ^{9}Li nucleus in the n^8Li channel in the energy range from 10^{-5} eV to 5 MeV based on E1 and *M*1 transitions. The experimentally proved resonance at $E_{c.m.}$ = 0.232 MeV in the $^4P_{5/2}$ wave and *ab initio*-predicted $^4P_{3/2}$ resonance at 1.32 MeV [Phys. Rev. C 103, 035801 (2021)] are considered. The strong impact of the asymptotic constant and channel spectroscopic factors on the total capture cross sections are responsible for the variation in the absolute values within factor two. As a consequence, the thermal cross sections are σ_{therm} = 24–46.8 mb. The evaluation of σ_{therm} based on the extrapolation of *ab initio* cross sections yields ~85 mb. The reaction rate is calculated in the temperature range from 0.01 to 10 T_9. The reported reaction rates are compared at the benchmark point 1 T_9. The comparison of two datasets [Phys. Rev. C 103, 035801 (2021) and Phys. Rev. C 105, 064608 (2022)] on reaction rates recently calculated in microscopic models in extended temperature intervals shows the essential quantitative and qualitative differences. The comparative joint analysis of the reaction rates of radiative neutron capture on the lithium isotopes ^{6,7,8}Li is suggested for the choice of an optimal interval for the asymptotic constants.

KEYWORDS

nuclear astrophysics, thermal and astrophysical energies, n^8Li system, total cross sections, reaction rate, cluster model

1 Introduction

The implication of an ^{8}Li$(n,\gamma)^9$Li reaction is under discussion since it was included in the following primordial nucleosynthesis chain suggested by Mao and Champagne (1991) and Kajino (1995):

$$\ldots{}^7\mathrm{Li}(n,\gamma)^8\mathrm{Li}(n,\gamma)^9\mathrm{Li}(\alpha,n)^{12}\mathrm{B}(\beta^+)^{12}\mathrm{C}\ldots. \quad (1)$$

The experimental study of the ^{8}Li$(n,\gamma)^9$Li reaction performed using the Coulomb dissociation method reported by Zecher et al. (1998) is still the only study since 1998 and provides only two cross-section points. The promising prospect for new experimental measurements is reported in the recent proposal of the study of the breakup of ^{9}Li on a ^{208}Pb target at a different energy regime (Gupta et al., 2022). This process is included in one of the chains of primordial nucleosynthesis.

Since this reaction plays a bridge role from the synthesis of light-seed nuclei A ≤ 7 to the heavy elements, theoretical model calculations are in high demand. The early theoretical calculations of cross sections and reaction rates presented by Malaney et al. (1988), Mao and Champagne (1991), Thielemann et al. (1991), Descouvemont (1993), Rauscher et al. (1994), Bertulani (1999), Kobayashi et al. (2003), Li et al. (2005), Guimarães et al. (2007), Banerjee et al. (2008), and Ma et al. (2012) differ significantly from each other (see Table 6 in Section 7 for details). A modern investigation of the ^{8}Li(n,γ)^{9}Li reaction is provided by microscopic models by McCracken et al. (2021) and Dong et al. (2022).

It is important to note that along with the sequence (1), other branching options involving ^{8}Li are possible: for example, the chain ^{7}Li(n,γ)^{8}Li(α,n)^{11}B(n,γ)^{12}B(β^{+})^{12}C was suggested as a possible explanation for the production of A ≥ 12 nuclides, observed in very metal-poor stars (Paradellis et al., 1990). Paradellis et al. (1990) raised a series of studies of the ^{8}Li(α,n)^{11}B reaction, covering the test of an inhomogeneous Big Bang model (Cherubini et al., 2004), as well as C-N-O Big Bang nucleosynthesis (BBN) (Su-Qing et al., 2010) at temperatures T_9 = 0.5–1.2. The key role of the ^{8}Li(α,n)^{11}B reaction is recognized in the production of seed nuclei at T_9 = 2.5–5, later burnt to heavier elements via r-capture reactions, during type II supernova explosions (La Cognata and Del Zoppo, 2011). It is worth noting that the reaction ^{8}Li(α,n)^{11}B has been more extensively studied than the radiative neutron capture on ^{8}Li, but their rates differ from each other within an order of magnitude (Das et al., 2017; Mondal et al., 2022). Hence, the continuation of the ^{7}Li(n,γ)^{8}Li chain remains an open area of investigation, and further studies are needed. Specifically, there is no definitive conclusion regarding the comparability of the reaction rates for ^{8}Li(n,γ)^{9}Li and ^{8}Li(α,n)^{11}B during the crucial temperature range of a standard BBN from 0.1 to 1 T_9.

Present consideration of the ^{8}Li(n,γ)^{9}Li reaction is performed in the framework of the modified potential cluster model (MPCM) (Dubovichenko, 2015; Dubovichenko, 2019). This model is based on classifying discrete and continuum orbital states by Young diagrams {f}, which effectively includes the Pauli principle while constructing the corresponding wave functions. Our results (Dubovichenko and Dzhazairov-Kakhramanov, 2016) need to be considered due to our recent research on the ^{7}Li(n,γ)^{8}Li reaction (Burkova et al., 2021). It was suggested that for the ^{8}Li nucleus, it is necessary to use the Young diagram {431} instead of {44}, assumed previously in Dubovichenko and Dzhazairov-Kakhramanov (2016). Such a diagram changed the entire structure of forbidden and allowed states for the interaction potentials in the n + ^{8}Li channel. Therefore, we examined this effect while calculating the total cross sections and reaction rates. The low-lying resonance at J^{π} = 5/2^{-} at the energy E_x = 4.296(15) MeV is considered in comparison with our previous study (Dubovichenko and Dzhazairov-Kakhramanov, 2016).

Recently, the properties of ^{9}Li-bound states and low-lying resonances were studied within the no-core shell model with continuum (NCSMC) (McCracken et al., 2021). The authors note that the *ab initio*-calculated ^{7}Li(n,γ)^{8}Li total cross section at the energies 20 keV to 1.6 MeV in the center-of-mass reference frame is nearly a factor two higher than that of our previous result (Dubovichenko and Dzhazairov-Kakhramanov, 2016). In the present work, we explain the origin of this discrepancy and come to an acceptable agreement with McCracken et al. (2021). The results of the low-temperature reaction rates at T_9 < 1 still remain in question.

Radiative neutron capture reaction rates on ^{6,7,8}Li nuclei are compared to estimate the "neutron poisoning" lithium isotope destruction.

This work is organized as follows: Section 2 presents the main aspects of the MPCM. Section 3 covers calculation methods. Classification of orbital states and interaction potentials are given in Section 4 and Section 5, respectively. Section 6 presents the total cross sections. Reaction rates are provided in Section 7. The conclusion is given in Section 8.

2 A brief review of the MPCM

The MPCM has been used to calculate the astrophysical S-factor and total cross section of a number of reactions (Dubovichenko, 2015; Dubovichenko, 2019), also employing the classification of orbital states according to the Young diagrams (Nemets et al., 1988; Neudatchin et al., 1992). The main feature of the MPCM is the concept of states forbidden by the Pauli principle, which are orthogonal to the allowed states. The interaction potentials are constructed to fit this orthogonality condition (Dubovichenko and Uzikov, 2011). The evident success of the MPCM in describing the total cross sections of 40 radiative capture reactions is proved, under the assumption of two-body clustering both in initial and final channels, in monographs (Dubovichenko, 2015; Dubovichenko, 2019) and reviews (Dubovichenko and Dzhazairov-Kakhramanov, 2017).

The MPCM was introduced in one of our papers about 10 years ago [see (Dubovichenko et al., 2013)], but in terms of meaning and calculation methods, we have operated with this model since the 1980s (Dubovichenko and Zhusupov, 1984a; Dubovichenko and Zhusupov, 1984b; Dubovichenko and Dzhazairov-Kakhramanov, 1990; Dubovichenko et al., 1990). It is important to note that the first classification of cluster states, according to Young diagrams, was introduced in the works of V. G. Neudatchin et al. in the early 1970s (Neudatchin et al., 1971; Neudatchin et al., 1972). We extended this theory to other light nuclei with A ≤ 8 (Itzykson and Nauenberg, 1966; Dubovichenko, 1997).

The basic principles of the MPCM are formulated in an extended version in recent papers (Dubovichenko et al., 2022a; Dubovichenko et al., 2023a). In summary, the MPCM is a two-particle model that accounts for the internal characteristics of clusters, such as their sizes, charges, and masses. The Pauli principle is implemented via the exclusion of the forbidden states, manifesting in proper node behavior of the radial wave function. Potentials of the bound states are constructed based on asymptotic constants and binding energies. Potentials of the scattering processes are built based on the spectra of the final nucleus or the scattering phase shifts of the particles of the input channel. Parameters of the potentials are fixed or variable within the asymptotic constant error intervals and vary within the energy or width errors of resonant or excited states. The radial wave functions of both continuous and discrete states are constructed to match the appropriate asymptotic behaviors.

3 Calculation methods

We use well-known formulas for the total cross sections and matrix elements for the operators of electromagnetic *NJ* transitions (Dubovichenko, 2015; Dubovichenko, 2019). These expressions are given in reviews (Angulo et al., 1999; Dubovichenko, 1997):

$$\sigma\left(NJ,J_f\right)=\frac{8\pi Ke^2}{\hbar^2k^3}\frac{\mu}{(2S_1+1)(2S_2+1)}\frac{J+1}{J[(2J+1)!!]^2}A_J^2(NJ,K)\times\sum_{L_i,J_i}P_J^2\left(NJ,J_f,J_i\right)I_J^2\left(k,J_f,J_i\right). \tag{2}$$

The matrix elements of convection electric *EJ* transitions have the following form:

$$P_J^2\left(EJ,J_f,J_i\right)=\delta_{S_iS_f}\left[(2J+1)(2L_i+1)(2J_i+1)\left(2J_f+1\right)\right]\left(L_i0J0\middle|L_f0\right)^2\left\{\begin{matrix}L_i & S & J_i\\ J_f & J & L_f\end{matrix}\right\}^2, \tag{3}$$

$$A_J(EJ,K)=K^J\mu^J\left(\frac{Z_1}{m_1^J}+(-1)^J\frac{Z_2}{m_2^J}\right), \tag{4}$$

$$I_J\left(k,J_f,J_i\right)=\langle\chi_f|r^J|\chi_i\rangle. \tag{5}$$

The spin part of the magnetic dipole process $M1(S)$ at $J=1$ is defined as

$$P_1^2\left(M1,J_f,J_i\right)=\delta_{S_iS_f}\delta_{L_iL_f}\left[S(S+1)(2S+1)(2J_i+1)\left(2J_f+1\right)\right]\left\{\begin{matrix}S & L & J_i\\ J_f & 1 & S\end{matrix}\right\}^2, \tag{6}$$

$$A_1(M1,K)=\frac{\hbar K}{m_0c}\sqrt{3}\left[\mu_1\frac{m_2}{m}-\mu_2\frac{m_1}{m}\right], \tag{7}$$

$$I_J\left(k,J_f,J_i\right)=\langle\chi_f\left|r^{J-1}\right|\chi_i\rangle. \tag{8}$$

The notations in Eqs 2–8, i.e., S_i, S_f, L_f, L_i, J_i, and J_f, are the spins, orbital, and total angular momentums in the initial (i) and final (f) channels; m_1, m_2, Z_1, and Z_2 are the masses and charges of the particles of the initial channel; I_J is the integral over the radial wave functions of initial χ_i and final χ_f states, and the radial part of the multiple operators; $m=m_1+m_2$; and μ_1 and μ_2 are the magnetic moments of the clusters.

The neutron mass $m_1=m_n=1.00866491597$ amu (NIST, 2019), and the ^{8}Li mass is $m_2=m_{^8\mathrm{Li}}=8.022487$ amu (Varlamov et al., 2015). The magnetic moments in nuclear magnetons μ_0 are $\mu(^8\mathrm{Li})=1.653560\mu_0$ (Neugart et al., 2008) and $\mu_n=-1.91304272\mu_0$ (NIST, 2019).

The radial scattering and bound state functions χ_i and χ_f in the overlap integrals $I_J(k,J_f,J_i)$ defined by Eqs 5, 8 are the numerical solutions of the Schrödinger equation. For the bound states, we use the following asymptotical analytical representation via the dimensionless constant C_w, determined by Plattner and Viollier (1981):

$$\chi_L(r)=\sqrt{2k_0}C_wW_{-\eta L+1/2}(2k_0r). \tag{9}$$

$W_{\eta L+1/2}$ is the Whittaker function, k_0 is the wavenumber related to the channel binding energy, η is the Sommerfeld parameter (here, $\eta=0$ since we are talking about neutrons), and L is the orbital momentum of the given bound state.

The asymptotic normalization coefficient (ANC) A_{NC} is related to the experimental asymptotic constant C by the following expression (Mukhamedzhanov and Tribble, 1999):

$$A_{\mathrm{NC}}=\sqrt{S_f}C, \tag{10}$$

where S_f is the spectroscopic factor and C is the dimensional asymptotic constant (AC), which is also represented in terms of the asymptotic wave functions:

$$\chi_L(r)=CW_{-\eta L+1/2}(2k_0r) \tag{11}$$

For a continuous spectrum, $\chi_L(r)$ found by numerical methods is matched with asymptotics of another form, which generally depends on Coulomb functions but on Riccati–Bessel functions if the Sommerfeld parameter $\eta=0$ (Dubovichenko and Dzhazairov-Kakhramanov, 2015).

The calculating methods of other quantities within the framework of the MPCM, i.e., root-mean mass and charge radii or binding energy, are given, for example, in our works (Dubovichenko, 2015; Dubovichenko, 2019; Dubovichenko and Dzhazairov-Kakhramanov, 2015). The energies of bound states are searched for by the finite difference method outlined by Dubovichenko (2012), Dubovichenko (2015), and Dubovichenko (2019). One can use the variational method to control the correctness of these energies, and such a procedure has been used, for example, by La Cognata and Del Zoppo (2011), Das et al. (2017), and in Supplementary Appendix SA of the study by Dubovichenko and Dzhazairov-Kakhramanov (2015). It should be noted that the accuracy of searching for the binding energy by these methods in some cluster systems can reach up to 10 meV or 0.01 eV (Dubovichenko et al., 2017). The calculation details for a number of cluster systems are presented in books (La Cognata and Del Zoppo, 2011; Das et al., 2017) and reviews (Neudatchin et al., 1992; Tilley et al., 2002; Dubovichenko, 2012; Dubovichenko and Dzhazairov-Kakhramanov, 2015; Sukhoruchkin and Soroko, 2016; Dubovichenko et al., 2017; Burkova et al., 2021).

4 Classification and structure of ^{9}Li states

For the ^{8}Li nucleus, as shown by Burkova et al. (2021), we consider the Young orbital diagram (431), so for the n^8Li system, we consider {431} × {1} = {531} + {441} + {432}. The diagram {531} corresponds to $L=1$, 2, and 3 and is forbidden since the *s*-shell cannot contain five nucleons (Neudatchin et al., 1992). Allowed diagrams {441} and {432} may be put in compliance with the GS of the ^{9}Li nucleus in the n^8Li channel alone with the orbital angular momentum $L=1$. Following Neudatchin et al. (1992), the scattering states turn out to be mixed by {441} + {432} diagrams, while the bound states refer only to the {441} diagram. It should be noted that forbidden states appear as bound only in both discrete and continuous spectra.

To reconstruct the GS total angular momentum, parity, and isospin J^π, T = 3/2$^-$, 3/2 of ^{9}Li, we used the ^{8}Li data J^π, T = 2$^+$, 1 obtained by Tilley et al. (2002). The spin channel $n+^8$Li is defined by the vector addition of ^{8}Li and n total spins, i.e., $\boldsymbol{S}=\mathbf{2}+\mathbf{1/2}$, and allows two states $S=3/2$ and $S=5/2$. Therefore, a spin-mixed $^{4+6}P_{3/2}$

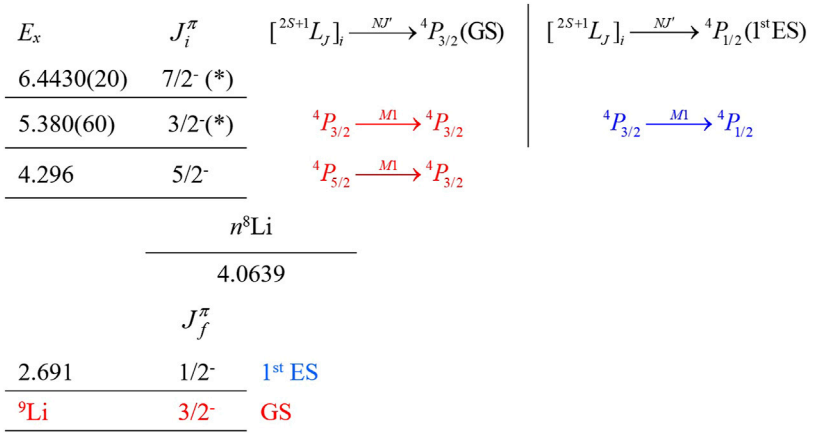

FIGURE 1
Energy spectrum of ^{9}Li in MeV (Tilley et al., 2002; Sukhoruchkin and Soroko, 2016). Data (*) comprise the *ab initio* prediction of McCracken et al. (2021).

TABLE 1 Multipole transitions to GS and first ES of the ^{9}Li nucleus in the n^8Li channel and coefficients $P_J^2(NJ, J_f, J_i)$ from Eqs 3, 6.

No.	$(^{2S+1}L_J)_i$	NJ transition	$(^{2S+1}L_J)_f$	$P_J^2(NJ, J_f, J_i)$
1	${}^4S_{3/2}$	$E1$	${}^4P_{3/2}$	4
2	${}^4P_{1/2}$	$M1$	${}^4P_{3/2}$	10/3
3	${}^4P_{3/2}$	$M1$	${}^4P_{3/2}$	121/15
4	${}^4P_{5/2}$	$M1$	${}^4P_{3/2}$	18/5
6	${}^4S_{3/2}$	$E1$	${}^4P_{1/2}$	2
7	${}^4P_{1/2}$	$M1$	${}^4P_{1/2}$	25/6
8	${}^4P_{3/2}$	$M1$	${}^4P_{1/2}$	10/3

state is possible for the GS (in the spectral notation $^{2S+1}L_J$), but we consider it a pure ${}^4P_{3/2}$ state. There is only one excited state at an energy of 2.691(5) MeV relative to the GS and binding energy $E_b = -1.3729(5)$ MeV. The first excited state (1st ES) with $J^\pi = 1/2^-$ is assumed a ${}^4P_{1/2}$ state.

Figure 1 illustrates the spectrum of the ^{9}Li nucleus in the n^8Li channel. The reliable, experimentally confirmed complete data on the total angular momentum, parity, excitation energy E_x, and width $\Gamma_{c.m.}$ are known for the first resonant state only (Tilley et al., 2002; Sukhoruchkin and Soroko, 2016).

This state with $J^\pi = 5/2^-$ is located at an excitation energy $E_x = 4.296(15)$ MeV relative to GS or 0.232(15) MeV relative to the threshold energy E_{th} of the n^8Li channel. Such a state is considered as a quartet ${}^4P_{5/2}$ wave. Dubovichenko (2012) and Dubovichenko et al. (2017)reported the width $\Gamma_{c.m.} = 100(30)$ keV. Based on these data, it is possible to construct a completely unambiguous ${}^4P_{5/2}$ elastic scattering potential with a bound forbidden state. The variations in potential parameters may come only within the accuracy of the resonance width.

The second excited state at $E_x = 5.38(6)$ MeV [1.32(6) MeV above E_{th}] with the width $\Gamma_{c.m.} = 600(100)$ keV is identified as a $3/2^-$ state in recent works (McCracken et al., 2021). For the third excited state, experimental data provide a value of E_x at 6.430(15) MeV and $\Gamma_{c.m.} = 40(20)$ keV, but the total angular momentum and parity $7/2^-$ were only predicted by McCracken et al. (2021). We consider the strong $E1$ and $M1$ transitions as the estimation of $E2$ transition shows its minor role (Dubovichenko and Dzhazairov-Kakhramanov, 2016).

Table 1 presents all treated transitions to the ground and first excited states of ^{9}Li in the n^8Li channel and $P_J^2(NJ, J_f, J_i)$ coefficients—Eqs 3, 6. The $E1$ dipole capture occurs from the ${}^4S_{3/2}$ scattering wave to the ${}^4P_{3/2}$ GS of ^{9}Li. Since we assume that the potentials depend on the Young diagrams, the scattering and bound states have different sets of Young diagrams, and transitions between states with the same angular momentums are allowed.

5 Interaction potentials

To construct the interaction potentials for the scattering states, we used the resonant-state parameters E_x, $\Gamma_{c.m.}$, and J^π. Non-resonant waves are provided by the potentials leading to the phase shifts close to zero (if there are no forbidden states), or to 180° if such a state appears in the classification of orbital states according to the Young diagrams.

The parameters of bound state potentials are conditioned by reproducing the data on the binding energy, matter, and charge radii, and the asymptotic constant (Dubovichenko, 2015; Dubovichenko, 2019; Dubovichenko and Dzhazairov-Kakhramanov, 2015).

The nuclear two-body interaction potential is represented as a Gaussoid (Dubovichenko, 2015; Dubovichenko, 2019):

$$V(r, SLJ, \{f\}) = -V_0(SLJ, \{f\}) \exp[-\alpha(SLJ, \{f\})r^2]. \quad (12)$$

5.1 Continuous spectrum

The potential parameters of Eq. 12 are listed in Table 2. These reproduce well the data on the ${}^4P_{5/2}$ and ${}^4P_{3/2}$ resonant states (Tilley et al., 2002; Sukhoruchkin and Soroko, 2016). As for the non-resonant-state ${}^4P_{1/2}$, the corresponding potential is deep enough

TABLE 2 Parameters of interaction potentials of n + ^{8}Li continuum.

No.	$(^{2S+1}L_J)_i$	V_0, MeV	α, fm^{-2}	E_{res}, keV	$\Gamma_{c.m.}$, keV
1	$^4P_{5/2}$	240.87	0.3	230 (1)	109 (1)
2	$^4P_{3/2}$	1,608.185	2.0	1,320 (10)	608 (10)
3	$^4P_{1/2}$	520.0	1.0	—	—
4	$^4S_{3/2}$	20.0	1.0	—	—

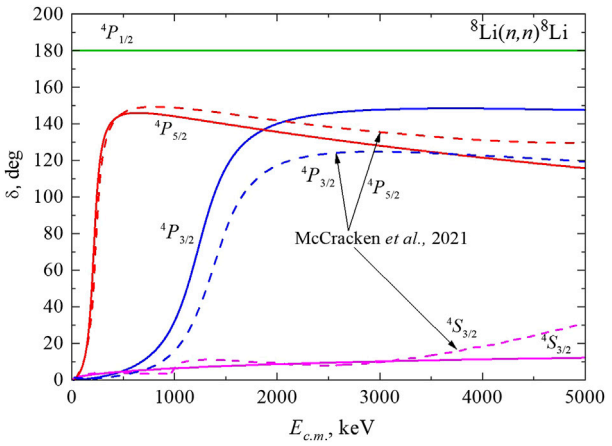

FIGURE 2
Phase shifts of elastic n^8Li scattering: solid curves are the results of MPCM calculations with the potential parameters given in Table 2; dashed curves are *ab initio* results obtained by McCracken et al. (2021) (digitalized).

to include the forbidden state. The *S*-wave does not appear in the ^{9}Li spectrum neither as the bound state nor as the resonant state. Therefore, the corresponding potential in Table 2 might lead to zero or near-zero phase shifts.

The corresponding calculated phase shifts are shown in Figure 2. The $\delta_{^4P_{5/2}}$ and $\delta_{^4P_{3/2}}$ phase shifts reveal the resonant energy dependence. The non-resonant $\delta_{^4P_{1/2}}$ phase shift corresponds to the potential with the forbidden state no. 3 given in Table 2. In accordance with the generalized Levinson theorem, this phase shift starts from 180° (Neudatchin et al., 1992). For the non-resonant $^4S_{3/2}$ scattering wave, the parameter no. 4 in Table 2 is found, and the corresponding $\delta_{^4S_{3/2}}$ phase shift shows smooth energy dependence, as shown in Figure 2.

The comparison between phase shifts obtained in the MPCM and *ab initio* NCSMC calculations [digitalized data obtained by McCracken et al. (2021)] is shown in Figure 2. Phase shifts $\delta_{^4P_{5/2}}$ illuminate rather well the agreement of both models within ~10° at the energies following the resonance at 230 keV. $\delta_{^4S_{3/2}}$ phase shifts are also very close up to ~3,500 keV, and the difference rises up to ~20° at the edge of the treated energy interval $E_{c.m.}$ = 5 MeV. The visual distinction is observed in the energy dependence of $\delta_{^4P_{3/2}}$ shifts, both in the resonance position and in the whole energy range. In advance, we may state that the $^4P_{3/2}$ wave provides a second very wide resonance at 1.320 MeV in cross sections via *M*1 transition and plays a moderate role (see Section 7).

5.2 Discrete spectrum

The following data on the ANC are considered to build the GS potential. The experimental values are deduced from the data on the neutron transfer reaction ^{8}Li(d,p)^{9}Li$_{g.s.}$ obtained by Guimarães et al. (2006). A_{NC} = 0.96(8) fm$^{-1/2}$, and in the study by Tilley et al. (2002), A_{NC} = 1.15(14) fm$^{-1/2}$. Their average value A_{NC} = 1.06(10) fm$^{-1/2}$ agrees with the results obtained by Timofeyuk (2013), who reported a calculated value of 1.08 fm$^{-1/2}$ for A_{NC} GS. Timofeyuk (2013) also provided theoretical values of the spectroscopic factors 0.6 and 1.1 obtained by two methods, which correspond to an average value of S_f = 0.85(25). Other data on the spectroscopic factors are given in Table 3.

Estimation within the aforementioned limits for A_{NC} = 0.88–1.29 fm$^{-1/2}$, and the range for the spectroscopic factor S_f = 0.44–1.03 (Table 3) results in C_w = 0.95–2.03. In recent *ab initio* extended network calculations, A_{NC} = 1.23(6) fm$^{-1/2}$ was reported, along with spectroscopic factors S_f = 0.83–1.06 (Mukhamedzhanov and Timofeyuk, 1990). At the edges of these intervals, we obtain C_w = 1.30–1.42.

Huang et al. (2010) and Sargsyan et al. (2022)obtained, for the first ES of the ^{9}Li nucleus, A_{NC} = 0.4 fm$^{-1/2}$ (unfortunately, no uncertainties are available) at S_f = 0.55, which leads to C = 0.54 fm$^{-1/2}$ or the dimensionless constant C_w = 0.77 at S_f = 0.698.

In CDFE (2023) for GS, the calculations yield A_{NC} = 1.140(13) fm$^{-1/2}$, and for the first ES, A_{NC} = 0.308(7) fm$^{-1/2}$, which leads to C_w = 0.60(1) at S_f = 0.55. Timofeyuk (2013) reported, for the first ES, A_{NC} = 0.33 fm$^{-1/2}$ at $\bar{S}_f$ = 0.38(6), which yields C_w = 0.76(4).

The potential parameters for the bound ground and excited states of the ^{9}Li in n^8Li channel are summarized in Table 4. In the present calculations, we use an ^{8}Li radius equal to 2.327 ± 0.0298 fm (Sánchez et al., 2007). The radius of ^{9}Li is 2.2462 ± 0.0315 fm (Sánchez et al., 2007). Nörtershäuser et al. (2005)used radii values 2.299(32) fm for ^{8}Li and 2.217(35) fm for ^{9}Li. Dubovichenko et al. (2022b) obtained, for these radii, 2.30(4) fm and 2.24(4) fm. The neutron charge radius is assumed to be zero, and the mass radius of 0.8414 fm coincides with the known proton radius (NIST, 2019).

The upper and lower sets refer to the GS and first ES interaction potentials, respectively, defined in Table 4, and differ by the C_w values but lead to the same binding channel energy.

6 Total cross sections of radiative n^8Li capture

The results of the present calculation of the integral total and partial cross sections are shown in Figure 3A. Strong sensitivity on the C_w values is observed for the upper and lower sets. The input of the first ES into the total cross sections is negligible if compared with that of the GS in both cases. The dipole electric *E*1 transition from the $^4S_{3/2}$ wave to $^4P_{3/2,\ 1/2}$ bound states provides low-energy cross sections and serves as a base for the resonant magnetic *M*1 transitions. Both resonances $^4P_{5/2}$ and $^4P_{3/2}$ are present at the energies ~230 keV and 1.32 MeV.

The comparison of the cross sections calculated in the MPCM and within the microscopic models (McCracken et al., 2021; Dong et al., 2022), along with the experimental data (Zecher et al., 1998), is shown in Figure 3B. The red band is obtained by varying C_w between

TABLE 3 Spectroscopic factors for the GS of ^{9}Li in the n + ^{8}Li channel from the studies by Li et al. (2005), Wuosmaa et al. (2005), Kanungo et al. (2008), and Wiringa (2021).

Reference	Reaction from which S_f is determined	Spectroscopic factor for n + $^8Li_{GS}$
Li et al. (2005)	^{8}Li(d,p)^{9}Li	0.68 (14)
Wuosmaa et al. (2005)	^{2}H(^{8}Li,p)^{9}Li	0.90 (13)
Wiringa (2021)	^{9}Be(^{8}Li, ^{9}Li) ^{8}Be	0.62 (7)
Kanungo et al. (2008)	d(^{9}Li,t)^{8}Li	0.65 (15)
Kanungo et al. (2008)	d(^{9}Li,t)^{8}Li	0.59 (15)
	Value interval	0.44–1.03
	Mean value	0.74 (30)

Note that in *ab initio* calculations, the value of the GS spectroscopic factor is equal to 0.99 (Huang et al., 2010), which is close to the results obtained by Blokhintsev et al. (1990), Mukhamedzhanov and Timofeyuk (1990), Nollett and Wiringa (2011), Timofeyuk (2013), Sargsyan et al. (2022), and CDFE (2023). They are all in agreement within the errors.

TABLE 4 Parameters of the bound ground and excited state potentials of the ^{9}Li in n+^{8}Li channel and calculated asymptotic constant C_w, R_{ch}, and R_m radii, and binding energy E_b.

No.	$(^{2S+1}L_J)_i$	V_0, MeV	α, fm^{-2}	C_w	R_{ch}, fm	R_m, fm	E_b, MeV	Set
1	$^4P_{3/2}$, GS	295.28320	0.33	1.40(1)	2.36	2.43	4.06390	Upper
2	$^4P_{3/2}$, GS	600.07219	0.70	0.93(1)	2.35	2.35	4.06390	Lower
3	$^4P_{1/2}$, 1st ES	295.6387	0.35	0.77(1)	2.37	2.37	1.37290	Upper
4	$^4P_{1/2}$, 1st ES	581.05205	0.07	0.58(1)	2.36	2.36	1.37290	Lower

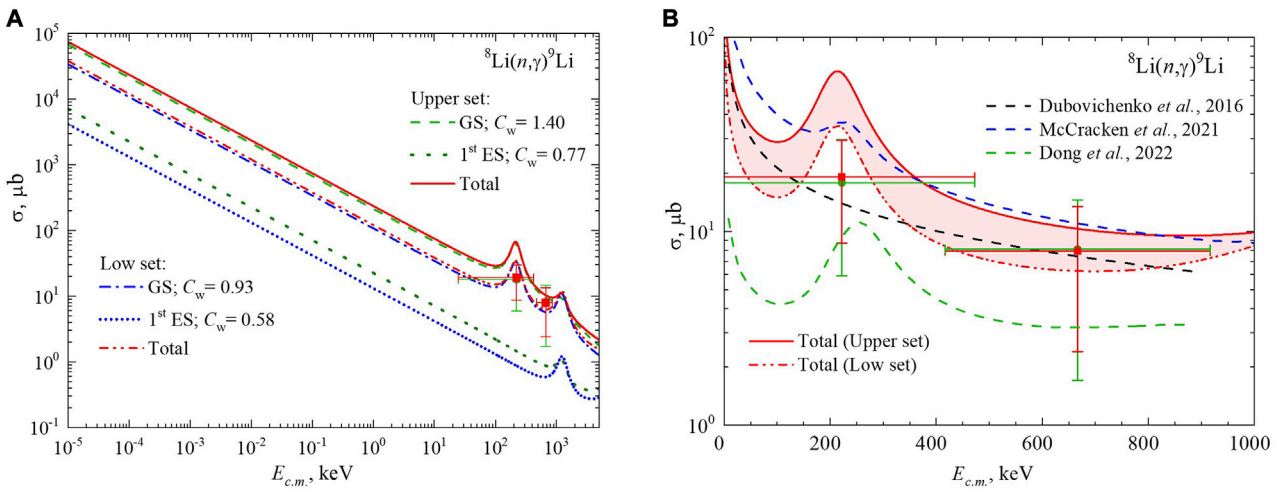

FIGURE 3
Total cross sections of radiative ^{8}Li(n,γ)^{9}Li capture in the GS and first ES of the ^{9}Li nucleus. Experimental data on ^{9}Li Coulomb dissociation obtained by Zecher et al. (1998): green dots on the Pb target and red squares on the U target. **(A)** MPCM calculations are explained in the legend. **(B)** Comparison of the MPCM and microscopic calculations: present MPCM total cross sections are the same as in panel **(A)**, the blue dashed curve shows the *ab initio* results obtained by McCracken et al. (2021), and the green dashed curve shows the results obtained by Dong et al. (2022) (digitalized). The black dashed curve shows our previous results obtained by Dubovichenko and Dzhazairov-Kakhramanov (2016).

0.93 and 1.4. The results on σ(E) obtained by Dong et al. (2022) differ essentially in the whole energy range and reach the lower error bar limits only. Therefore, it is more reasonable to compare the MPCM and *ab initio* results obtained by McCracken et al. (2021). The difference is observed at the energies close to the first resonance $^4P_{5/2}$: the lower set (red dash-double-dotted curve) and *ab initio* cross sections (blue dashed curve) are comparable, contrary to the upper set application (red solid curve). Out of the resonance range $E_{c.m.}$ > 300 keV and up to 1 MeV, the upper set and *ab initio* cross sections practically coincide and fit the second experimental point fairly well. The low-energy cross-section part is discussed in the following sections.

TABLE 5 Evaluated thermal cross sections in the n + ^{8}Li channel.

Reference	E_{min}, keV	$\sigma(E_{min})$, μb	A, μb·keV$^{1/2}$	σ_{therm}, mb
Present, upper set	10^{-5}	74,485.75	235.54	46.8
Present, lower set	10^{-5}	38,179.97	120.74	24.0
McCracken et al. (2021)	20	95.125	425	85
Dong et al. (2022)	8.55	11.58	33.86	6.7
Descouvemont (1993)	25	38	190	37.9

The total capture cross section of thermal and cold neutrons shows the following energy dependence (Dubovichenko, 2015; Dubovichenko, 2019):

$$\sigma_{ap}(\mu b) = \frac{A}{\sqrt{E(keV)}}. \quad (13)$$

Based on one available point, the $\sigma(E_{min})$ constant A(μb·keV$^{1/2}$) is determined, and calculation of the thermal cross section at 25.3 meV may be implemented according to Eq. 13. The results on σ_{therm} obtained in the present work and recalculated with data obtained by McCracken et al. (2021) and Dong et al. (2022) are presented in Table 5, as well as the value obtained by Descouvemont (1993). In our previous work, we observed σ_{therm} = 41.3 (1) mb (Dubovichenko and Dzhazairov-Kakhramanov, 2016). The accuracy of approximation (Eq. 13) is approximately 0.6% and 0.7% for the upper and lower sets, respectively.

A comparison between various σ_{therm} values shows that our upper set results are in agreement with the data obtained in RGM by Descouvemont (1993). Both these values are comparable with thermal cross sections for the neutron capture on ^{6}Li and ^{7}Li calculated in MPCM. Firestone and Revay (2016) reported theoretical values of σ_{therm} = 39.7 mb for n + ^{6}Li and σ_{therm} = 44.2 mb for n + ^{7}Li (Burkova et al., 2021). The results on ^{6}Li and ^{7}Li are in excellent agreement with experimental data (Iliadis, 2015). Therefore, in the context of this background, the results of works (McCracken et al., 2021; Dong et al., 2022) on σ_{therm} do not look consistent.

7 Reaction rate of radiative n^{8}Li capture

The well-known expression for the radiative neutron capture reaction rate in terms of the Maxwellian averaged cross sections is

$$N_A\langle\sigma v\rangle = 3.7313 \cdot 10^{4}\mu^{-1/2}T_9^{-3/2}\int_0^{\infty}\sigma(E)E\exp(-11.605E/T_9)dE, \quad (14)$$

where E is expressed in MeV, the total cross section $\sigma(E)$ is represented in μb, μ is the reduced mass in amu, and T_9 is the temperature in 10^9 K (Norman and Schramm, 1979). Based on the total cross sections shown in Figure 3A, the corresponding reaction rates are presented in Figure 4A. The band refers to the upper and lower sets of GS and first ES interaction potentials, as shown in Table 4, applied to calculate total cross sections. The temperature dependence of $N_A\langle\sigma v\rangle_{MPCM}$ shows near coherent behavior for the upper and lower C_w sets, with a moderate plateau transforming into a noticeable increase above 0.2–0.3 T_9 due to the resonance at 232 keV. The second resonance at 1.3 MeV is not observed. The capture to the first excited state may be regarded as a minor correction to the GS reaction rate.

A comparison of MPCM new results and calculations obtained by McCracken et al. (2021) and Dong et al. (2022), as well as our early data obtained by Dubovichenko and Dzhazairov-Kakhramanov (2016), is presented in Figure 4B. The *ab initio* reaction rate (McCracken et al., 2021) (blue dashed curve) exceeds our results at low temperatures and approximately coincides in the resonance region. A noticeable decrease in $N_A\langle\sigma v\rangle_{ab\,initio}$ is observed at $T_9 > 1$. This "falling effect" is explained in detail in Supplementary Appendix SA, where an approximation of the real calculation of the integral in Eq. 14 is performed by varying the upper E_{max} and low E_{min} limits. The *ab initio* cross section is calculated in the energy region $E_{c.m.}$ = 20 keV–1.6 MeV so that the energy interval extension will lead a reaction rate at $T_9 > 1$. We consider the equality of the "upper set" $N_A\langle\sigma v\rangle_{MPCM}$ and $N_A\langle\sigma v\rangle_{ab\,initio}$ at $T_9 \simeq 1$ in Figure 4B accidental. The great difference between reaction rates appears at $T_9 < 1$. Both model calculations MPCM and *ab initio* do not agree with the results obtained by Dong et al. (green dashed curve in Figure 4B) (Dong et al., 2022). Tabulated numerical data on the MPCM reaction rates and their analytical parametrization are provided in Supplementary Appendix SB.

Since 1988 (Malaney et al., 1988), significant efforts have been made to find the consensus on the reaction rate value at T_9 = 1, useful in the context of BBN. Table 6 shows the comparison of different results for the reaction rates, which are partially taken from the studies by Kobayashi et al. (2003), Banerjee et al. (2008), Dubovichenko and Dzhazairov-Kakhramanov (2016), and Dong et al. (2022).

We complemented the data on the reaction rates with the neutron number densities n_n, which may be referred to as the *r*-process *ignition threshold density* since it is calculated under the condition of equality of the ^{8}Li mean lifetime and neutron capture time $\tau_\beta \approx \tau(n,\gamma)$ following the general definitions of the Nuclear Data Evaluation Project (2021):

$$n_n = \frac{1}{\tau_\beta}\cdot\frac{1}{\langle\sigma_{n,\gamma}v\rangle}. \quad (15)$$

The isotope ^{8}Li is unstable with a half-life time $t_{1/2}$ = 838.79 ± 0.36 ms (Kajino et al., 2019) or τ_β = 1.186 s. The estimated neutron number densities n_n given in Table 6 condition the start of the

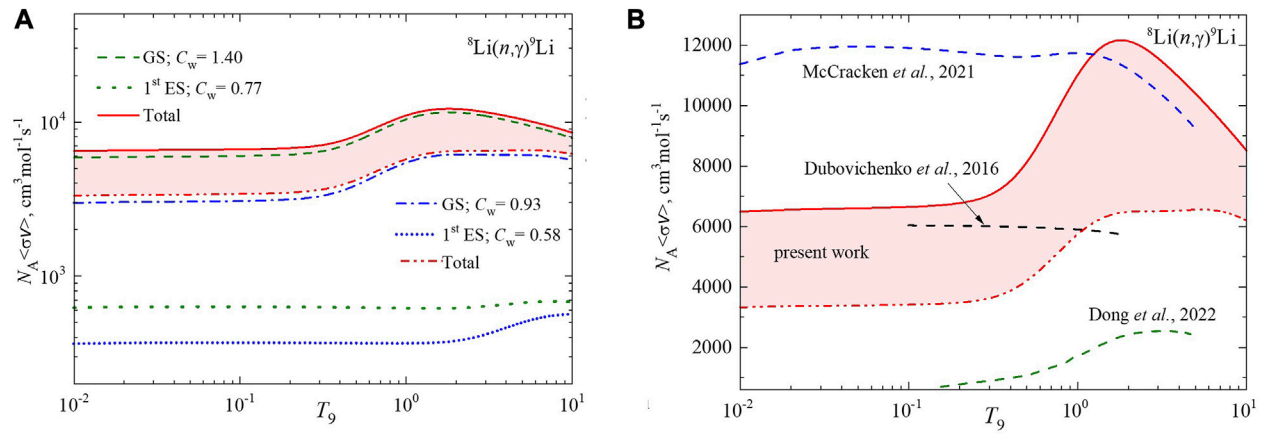

FIGURE 4
Reaction rate of radiative ^{8}Li(n,γ)^{9}Li capture to the GS and first ES of ^{9}Li. **(A)** MPCM calculations are explained in the legend. **(B)** Comparison of MPCM and microscopic calculations: present MPCM reaction rates are the same as in panel **(A)**, the blue dashed curve shows the *ab initio* results obtained by McCracken et al. (2021), and the green dashed curve shows the results obtained by Dong et al. (2022) (digitalized). The black dashed curve shows our previous results from Dubovichenko and Dzhazairov-Kakhramanov (2016).

TABLE 6 Comparison of reaction rates for the direct capture of the ^{8}Li(n,γ)^{9}Li reaction at T_9 = 1.

Reference	Reaction rate, cm^3·mol^{-1}·s^{-1}	Neutron number density, cm^{-3}
Experiment		
Zecher et al. (1998)	<7,200	6.9·10^{19}
Kobayashi et al. (2003)	<790	6.3·10^{20}
Li et al. (2005)	4,000	1.2·10^{20}
Guimarães et al. (2007)	3,270	1.5·10^{20}
Gupta et al. (2022)	<790	6.3·10^{20}
Theory		
Malaney et al. (1988)	43,000	1.2·10^{19}
Mao and Champagne (1991)	21,000	2.4·10^{19}
Thielemann et al. (1991)	3,350	1.5·10^{20}
Descouvemont (1993)	5,300	9.4·10^{19}
Rauscher et al. (1994)	4,500	1.1·10^{20}
Bertulani (1999)	2,200	2.3·10^{20}
Banerjee et al. (2008)	2,900	1.7·10^{20}
Ma et al. (2012)	<4,300	1.2·10^{20}
Dubovichenko and Dzhazairov-Kakhramanov (2016)	5,900	8.4·10^{19}
McCracken et al. (2021)	11,770	4.2·10^{19}
Dong et al. (2022)	1,479	3.4·10^{20}
Present, 2023	Up: 11,000	4.5·10^{19}
	Adopted: 8,370	5.9·10^{19}
	Low: 5,740	8.7·10^{19}

r-process on ^{8}Li at T_9 = 1 and lay in the interval 1.2·10^{19}–6.3·10^{20} cm^{-3}, which brings forth a difference of up to the factor 50 with respect to the listed datasets. Following the study by Dubovichenko et al. (2019), the typical conditions for the *r*-process n_n~3·10^{23} cm^{-3} and T_9~1 require both an explosive environment and high-density neutron-rich matter. In this context, the difference in the reaction rate data given in Table 6 seems not so crucial.

We still see a challenge in finding any cross-points that allow us to resolve the problem of variable ^{8}Li(n,γ)^{9}Li reaction rates. One point we assume is related to the thermal cross sections for the ^{6,7,8}Li isotopes discussed in Section 6 (Table 5). Another one is based on our experience of studying the radiative capture reaction rates on the

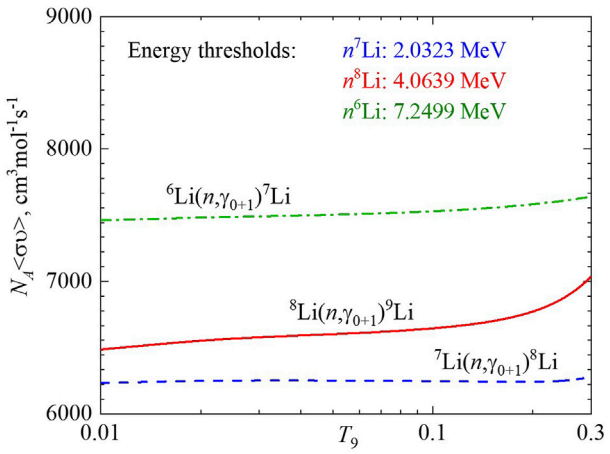

FIGURE 5
The reaction rates of radiative neutron capture for ^{6}Li(n,γ$_{0+1}$)^{7}Li (Firestone and Revay, 2016), ^{7}Li(n,γ$_{0+1}$)^{8}Li (Burkova et al., 2021), and ^{8}Li(n,γ$_{0+1}$)^{9}Li present results for the upper set in Figure 4. Threshold energies E_{th} are given in square brackets.

group of the neighboring isotopes. For example, it was found that low-temperature reaction rates for $^{10\text{-}13}$B$(n,\gamma)^{11\text{-}14}$B conditioned by the *S*-wave capture outside of the resonance energy region show some regularity—the higher the channel threshold, the higher the reaction rate (Dubovichenko et al., 2020; Dubovichenko et al., 2021; Dubovichenko et al., 2023a; Dubovichenko et al., 2023b). The same effect is observed for the proton capture on the nitrogen isotopes ^{12,13,15}N$(p,\gamma)^{13,14,16}$O (Kubono et al., 2016), and an exception is given by the reaction ^{14}N$(p,\gamma)^{15}$O as *S*-wave capture occurs via a weak *E*2 transition contrary to more advanced *E*1 or *M*1.

Figure 5 shows the reactions rates on lithium isotopes ^{6,7,8}Li calculated in the MPCM. We observe that the order of magnitude of $N_A\langle\sigma v\rangle$ below ~0.2 T_9 fits the threshold energy relation E_{th} (n^6Li) > E_{th} (n^8Li) > E_{th} (n^7Li) if, for the reaction ^{8}Li$(n,\gamma_{0+1})^9$Li, we take the upper set results. The reaction rates corresponding to the MPCM lower set, as well as *ab initio* calculations (McCracken et al., 2021), and data obtained by Dong et al. (2022) do not fit the aforementioned regularity. It must be underlined that the reactions ^{6}Li$(n,\gamma_{0+1})^7$Li (Firestone and Revay, 2016) and ^{7}Li$(n,\gamma_{0+1})^8$Li (Burkova et al., 2021) are examined much better as they directly concern the well-known *lithium problem* (Caughlan and Fowler, 1988; Coc, 2016).

8 Conclusion

Following our new results on the ^{7}Li$(n,\gamma_{0+1})^8$Li reaction (Burkova et al., 2021), we reconsider the reaction ^{8}Li$(n,\gamma_{0+1})^9$Li. The total cross sections and reaction rates are calculated for the reaction ^{8}Li$(n,\gamma_{0+1})^9$Li, including the corrections inserted for the interaction potentials comparing the early work (Dubovichenko and Dzhazairov-Kakhramanov, 2016).

The experimentally proved resonance at $E_{c.m.}$ = 0.232 MeV in the $^4P_{5/2}$ wave and *ab initio*-predicted $^4P_{3/2}$ resonance at 1.32 MeV (McCracken et al., 2021) are considered. The intensity of $^4P_{5/2}$ resonance depends strongly on the range of asymptotic constants C_w, as well as the cross sections as a whole, which is observed in the temperature T_9 dependence of the reaction rates.

The minor role of the (n,γ_1) process is proved; therefore, the GS transitions are dominant. The variation in the GS asymptotic constant C_w = 0.93–1.40 leads to the values of the reaction rate 5,740–11,000 cm^3·mol^{-1}·s^{-1} at temperature T_9 = 1 relevant for the *r*-formation of ^{9}Li. The upper value nearly coincides with the *ab initio* reaction rate 11,770 cm^3·mol^{-1}·s^{-1} at T_9 = 1 (McCracken et al., 2021), but we acknowledge this agreement as occasional.

We suggest two criteria to narrow down the range of reaction rates in our study. The first one concerns the values of thermal cross sections. Analysis of σ_{therm} values leads us to conclude that the upper set calculations yielding 46.8 mb (C_w = 1.40) are more relevant as they conform to estimations carried out by Descouvemont (1993) and data on the ^{6}Li and ^{7}Li isotopes (Iliadis, 2015).

The second criterion is related to the reaction rates of radiative neutron capture on lithium isotopes ^{6,7,8}Li. The examined correlation between the energy thresholds and order of reaction rates at low temperatures beyond the possible resonances T_9 < 0.2 leads to the conclusion that upper-set calculations are more reasonable (see Figure 5).

The recent results on the reaction rates obtained by McCracken et al. (2021) and Dong et al. (2022) show substantial differences, both qualitative and quantitative. The present calculations do not eliminate this discrepancy. The new measurements proposed by Gupta et al. (2022) may clarify the situation.

Data availability statement

The raw data supporting the conclusion of this article will be made available by the authors, without undue reservation.

Author contributions

All authors listed have made a substantial, direct, and intellectual contribution to the work and approved it for publication.

Funding

The work was supported by the grant of the Ministry of Education and Science of the Republic of Kazakhstan, No. AP09259021.

Acknowledgments

The authors sincerely thank P. Navratil for providing the numerical results on the cross section and reaction rate obtained by McCracken et al. (2021), and discussing some issues.

Conflict of interest

The authors declare that the research was conducted in the absence of any commercial or financial relationships that could be construed as a potential conflict of interest.

Publisher's note

Supplementary material

The Supplementary Material for this article can be found online at: https://www.frontiersin.org/articles/10.3389/fspas.2023.1251743/full#supplementary-material

References

Angulo, C., Arnould, M., Rayet, M., Descouvemont, P., Baye, D., Leclercq-Willain, C., et al. (1999). A compilation of charged-particle induced thermonuclear reaction rates. *Nucl. Phys. A* 656, 3–183. doi:10.1016/S0375-9474(99)00030-5

Banerjee, P., Chatterjee, R., and Shyam, R. (2008). Coulomb dissociation of ^{9}Li and the rate of the ^{8}Li(n,γ)^{9}Li reaction. *Phys. Rev. C* 78, 035804. doi:10.1103/PhysRevC.78.035804

Bertulani, C. A. (1999). The astrophysical reaction ^{8}Li(n,γ)^{9}Li from measurements by reverse kinematics. *J. Phys. G Nucl. Part. Phys.* 25, 1959–1963. doi:10.1088/0954-3899/25/9/313

Blokhintsev, L. D., Mukhamedzhanov, A. M., and Timofeyuk, N. K. (1990). The vertex constant of virtual decay $t\rightarrow d+n$ and a nucleon-nucleon potential. *Ukranian J. Phys.* 35, 341–345.

Burkova, N. A., Dubovichenko, S. B., Dzhazairov-Kakhramanov A, V., and Nurakhmetova, S. Z. (2021). Comparative role of the ^{7}Li(n,γ)^{8}Li reaction in Big Bang nucleosynthesis. *J. Phys. G Nucl. Part. Phys.* 48, 045201. doi:10.1088/1361-6471/abe2b5

Caughlan, G. R., and Fowler, W. A. (1988). Thermonuclear reaction rates V. *A. T. Data Nucl. Data Tables* 40, 283–334. doi:10.1016/0092-640X(88)90009-5

CDFE (2023). Chart of nucleus shape and size parameters. Available at: http://cdfe.sinp.msu.ru/cgi-bin/muh/radcard.cgi?z=3& a=9& td=123456 (Accessed June 1, 2023).

Cherubini, S., Figuera, P., Musumarra, A., Agodi, C., Alba, R., Calabretta, L., et al. (2004). 8Li(α,n)11B at big bang temperatures: neutron counting with a low intensity 8Li radioactive beamn. *AIP Conf. Proc.* 701, 68–72. doi:10.1063/1.1691688

Coc, A. (2016). Primordial nucleosynthesis. *J. Phys. Conf. Ser.* 665, 012001. doi:10.1088/1742-6596/665/1/012001

Das, S. K., Fukuda, T., Mizoi, Y., Ishiyama, H., Miyatake, H., Watanabe, Y. X., et al. (2017). New measurement of the ^{8}Li(α,n)^{11}B reaction in a lower-energy region below the Coulomb barrier. *Phys. Rev. C* 95, 055805. doi:10.1103/PhysRevC.95.055805

Descouvemont, P. (1993). The ^{8}Li(n,γ)^{9}Li and ^{8}B(p,γ)^{9}C mirror reactions in a microscopic cluster model. *Astrophys. J.* 405, 518. doi:10.1086/172383

Dong, G. X., Wang, X. B., Michel, N., and Płoszajczak, M. (2022). Gamow shell model description of the radiative capture reaction ^{8}Li(n,γ)^{9}Li. *Phys. Rev. C* 105, 064608. doi:10.1103/PhysRevC.105.064608

Dubovichenko, S., Dzhazairov-Kakhramanov, A., and Afanasyeva, N. (2013). Radiative neutron capture on ^{9}Be, ^{14}C, ^{14}N, ^{15}N and ^{16}O at thermal and astrophysical energies. *Int. J. Mod. Phys. E* 22, 1350075. doi:10.1142/S0218301313500754

Dubovichenko, S., and Dzhazairov-Kakhramanov, A. (2017). Study of the nucleon radiative captures ^{8}Li(n,γ)^{9}Li, ^{9}Be(p,γ)^{10}B, ^{10}Be(n,γ)^{11}Be, ^{10}B(p,γ)^{11}C, and ^{16}O(p,γ)^{17}F at thermal and astrophysical energies. *Int. J. Mod. Phys. E* 26, 1630009. doi:10.1142/S0218301316300095

Dubovichenko, S. B., Burkova, N. A., and Dzhazairov-Kakhramanov, A. V. (2019). Influence of low-lying resonances on reaction rates for ^{10}B(n,γ)^{11}B capture. *Nucl. Phys. A* 992, 121625. doi:10.1016/j.nuclphysa.2019.121625

Dubovichenko, S. B., Burkova, N. A., Dzhazairov-Kakhramanov, A. V., and Tkachenko, A. S. (2020). Influence of resonances on the ^{11}B(n,γ)^{12}B capture reaction rate. Capture to the ground state of ^{12}B. *Astropart. Phys.* 123, 102481. doi:10.1016/j.astropartphys.2020.102481

Dubovichenko, S. B., Burkova, N. A., Dzhazairov-Kakhramanov, A. V., and Yertaiuly, A. (2021). ^{12}B(n,γ)^{13}B reaction as an alternative path to astrophysical synthesis of ^{13}C isotope. *Nucl. Phys. A* 1011, 122197. doi:10.1016/j.nuclphysa.2021.122197

Dubovichenko, S. B., Burkova, N. A., Kezerashvili, R. Y., Tkachenko, A. S., and Yeleusheva, B. M. (2023b). The astrophysical S–factor and reaction rate for ^{15}N(p,γ)^{16}O within the modified potential cluster model. arXiv:2303.14680v2 [nucl-th].

Dubovichenko, S. B., Burkova, N. A., Tkachenko, A. S., and Dzhazairov-Kakhramanov, A. V. (2023a). Influence of resonances on the ^{11}B(n,γ)^{12}B reaction rate. Capture to the excited states of ^{12}B. *Int. J. Mod. Phys. E* 32. doi:10.1142/S0218301323500088

Dubovichenko, S. B., Burkova, N. A., and Tkachenko, A. S. (2022b). Reaction rate of radiative n^{6}Li capture in the temperature range from 0.01 to 10 T_9. *Nucl. Phys. A* 1027, 122520. doi:10.1016/j.nuclphysa.2022.122520

Dubovichenko, S. B., and Dzhazairov-Kakhramanov, A. V. (2016). The Reaction^{8}Li(n,γ)^{9}Li at Astrophysical Energies And Its Role In Primordial Nucleosynthesis. *Astrophys. J.* 819, 78. doi:10.3847/0004-637X/819/1/78

Dubovichenko, S. B., Dzhazairov-Kakhramanov, A. V., and Afanasyeva, N. V. (2017). New results for reaction rate of the proton radiative capture on ^{3}H. *Nucl. Phys. A* 963, 52–67. doi:10.1016/j.nuclphysa.2017.04.006

Dubovichenko, S. B., and Dzhazairov-Kakhramanov, A. V. (1990). Potential description of elastic *nd, dd, n*^{4}He, and *d*^{3}He scattering. *Soviet J. Nucl. Phys. USSR* 51, 971–977.

Dubovichenko, S. B., and Dzhazairov-Kakhramanov, A. V. (2015). Thermonuclear processes for three body system in the potential cluster model. *Nucl. Phys. A* 941, 335–363. doi:10.1016/j.nuclphysa.2015.07.009

Dubovichenko, S. B. (1997). Electromagnetic effects in light nuclei and the cluster potential model. *Phys. Part. Nucl.* 28, 615. doi:10.1134/1.953057

Dubovichenko, S. B. (2012). *Methods for calculating nuclear characteristics. Nuclear and thermonuclear processes*. Second edition. Saarbrucken, Germany: Lambert Acad. Publ., 425.

Dubovichenko, S. B., Neudachin, V. G., Sakharuk, A. A., and Smirnov, YuF. (1990). Generalized potential description of interaction of the hightest *pt* and *ph* nuclei. *Izv. Akad. Nauk. SSSR* 54, 911–916.

Dubovichenko, S. B. (2019). *Radiative neutron capture and primordial nucleosynthesis of the Universe*. First English edition. Berlin: De Gruyter, 310.

Dubovichenko, S. B. (2015). *Thermonuclear processes in stars and Universe*. Second Edition. Saarbrucken: Scholar's Press, 332.

Dubovichenko, S. B., Tkachenko, A. S., Kezerashvili, R. Y., Burkova, N. A., and Dzhazairov-Kakhramanov, A. V. (2022a). ^{6}Li(p,γ)^{7}Be reaction rate in the light of the new data of the Laboratory for Underground Nuclear Astrophysics. *Phys. Rev. C* 105, 065806. doi:10.1103/PhysRevC.105.065806

Dubovichenko, S. B., and Uzikov, Y. N. (2011). Astrophysical *S* factors of reactions with light nuclei. *Phys. Part. Nucl.* 42, 251–301. doi:10.1134/S1063779611020031

Dubovichenko, S. B., and Zhusupov, M. A. (1984a). Some characteristics of ^{7}Li in αt model for potentials with forbidden states. *Sov. Jour Nucl. Phys. USSR* 39, 1378–1381.

Dubovichenko, S. B., and Zhusupov, M. A. (1984b). The structure of light nuclei with A=6,7,8 in cluster models for potential with forbidden states. *Izv. Akad. Nauk. SSSR* 48, 935–937.

Firestone, R. B., and Revay, Z. (2016). Thermal neutron radiative cross sections for ^{6,7}Li, ^{9}Be, ^{10,11}B, ^{12,13}C, and ^{14,15}N. *Phys. Rev. C* 93, 054306. doi:10.1103/PhysRevC.93.054306

Guimarães, V., Camargo, O., Lichtenthaler, R., Barioni, A., Kolata, J. J., Amro, H., et al. (2006). "Investigation of nucleosynthesis capture reactions by using ^{8}Li radioactive beam transfer reactions," in Proceedings of International Symposium on Nuclear Astrophysics - Nuclei in the Cosmos - IX — PoS(NIC-IX), CERN, Geneva, 25-30 June 2006 (Trieste, Italy: Sissa Medialab). doi:10.22323/1.028.0108

Guimarães, V., Lichtenthäler, R., Camargo, O., Barioni, A., Assunção, M., Kolata, J. J., et al. (2007). Neutron transfer reactions induced by ^{8}Li on ^{9}Li. *Phys. Rev. C* 75, 054602. doi:10.1103/PhysRevC.75.054602

Guo, B., Li, Z. H., Liu, W. P., Bai, X. X., Lian, G., Yan, S. Q., et al. (2005). The ^{8}Li(d,p)^{9}Li reaction and astrophysical ^{8}B(p,γ)^{9}C reaction rate. *Nucl. Phys. A* 761, 162–172. doi:10.1016/j.nuclphysa.2005.07.013

Gupta, D., Kundalia, K., Ali, Sk M., and Mitra, R. (2022). *Break up of 9Li to study the 8Li(n,γ) reaction. European organization for nuclear research Proposal to the ISOLDE and Neutron Time-of-Flight Committee*.

Huang, J. T., Bertulani, C. A., and Guimarães, V. (2010). Radiative capture of nucleons at astrophysical energies with single-particle states. *A. T. Data Nucl. Data Tables* 96, 824–847. doi:10.1016/j.adt.2010.06.004

Iliadis, C. (2015). *Nuclear physics of stars*. Second. Weinheim, Germany: Wiley-VCH Verlag GmbH & Co. KGaA, 672.

Itzykson, C., and Nauenberg, M. (1966). Unitary groups: representations and decompositions. *Rev. Mod. Phys.* 38, 95–120. doi:10.1103/RevModPhys.38.95

Kajino, T., Aoki, W., Balantekin, A. B., Diehl, R., Famiano, M. A., and Mathews, G. J. (2019). Current status of *r*-process nucleosynthesis. *Prog. Part Nucl. Phys.* 107, 109–166. doi:10.1016/j.ppnp.2019.02.008

Kajino, T. (1995). Inhomogeneous big-bang model, revived, and evolution of the light elements in cosmic rays. *Nucl. Phys. A* 588, c339–c343. doi:10.1016/0375-9474(95)00159-X

Kanungo, R., Andreyev, A. N., Buchmann, L., Davids, B., Hackman, G., Howell, D., et al. (2008). Spectroscopic factors for the ^{9}Li ground state and N=6 shell closure. *Phys. Lett. B* 660, 26–31. doi:10.1016/j.physletb.2007.12.024

Kobayashi, H., Ieki, K., Horváth, Á., Galonsky, A., Carlin, N., Deák, F., et al. (2003). Astrophysical reaction rate for the ^{8}Li(n,γ)^{9}Li reaction. *Phys. Rev. C* 67, 015806. doi:10.1103/PhysRevC.67.015806

Kubono, S., Yamaguchi, H., Hayakawa, S., Hou, S. Q., and He, J. J. (2016). Explosive nuclear burning in the *pp*-chain region and the breakout processes. *EPJ Web Conf.* 109, 01001. doi:10.1051/epjconf/201610901001

La Cognata, M., and Del Zoppo, A. (2011). The ^{8}Li(α,n)^{11}B reaction rate at astrophysical temperatures. *Astrophys. J.* 736, 148. doi:10.1088/0004-637X/736/2/148

Li, Z. H., Liu, W. P., Bai, X. X., Guo, B., Lian, G., Yan, S. Q., et al. (2005). The ^{8}Li(d,p)^{9}Li reaction and the astrophysical ^{8}Li(n,γ)^{9}Li reaction rate. *Phys. Rev. C* 71, 052801. doi:10.1103/PhysRevC.71.052801

Ma, H-L., Dong, B-G., Yan, Y-L., and Zhang, X-Z. (2012). Shell model study on the astrophysical neutron capture of ^{8}Li. *Eur. Phys. J. A* 48, 125. doi:10.1140/epja/i2012-12125-3

R. A. Malaney, W. F. Fowler, and G. J. Matthews (Editors) (1988). *Origin and distribution of the elements* (Singapore: World Scientific).

Mao, Z. Q., and Champagne, A. E. (1991). The ^{8}Li(n,γ)^{9}Li reaction and primordial nucleosynthesis. *Nucl. Phys. A* 522, 568–577. doi:10.1016/0375-9474(91)90081-G

McCracken, C., Navrátil, P., McCoy, A., Quaglioni, S., and Hupin, G. (2021). Microscopic investigation of the ^{8}Li(n,γ)^{9}Li reaction. *Phys. Rev. C* 103, 035801. doi:10.1103/PhysRevC.103.035801

Mondal, S., Das, P., Senapati, E., Pandit, D., Dey, B., De, A., et al. (2022). Analysis of cross-section, S-factor and thermonuclear reaction rate of ^{8}Li(α,n)^{11}B and ^{14}N(p,γ)^{15}O using TALYS and EMPIRE nuclear reaction codes. *Int. J. Mod. Phys. E* 31. doi:10.1142/S0218301322500641

Mukhamedzhanov, A. M., and Timofeyuk, N. K. (1990). Microscopic calculation of nucleon separation vertex constant for 1*p* shell nuclei. *J. Soviet Nucl. Phys.* 51, 431–441.

Mukhamedzhanov, A. M., and Tribble, R. E. (1999). Connection between asymptotic normalization coefficients, subthreshold bound states, and resonances. *Phys. Rev. C* 59, 3418–3424. doi:10.1103/PhysRevC.59.3418

Nemets, O. F., Neudatchin, V. G., Rudchik, A. T., and Smirnov, Y. F.Tchuvil'sky YuM (1988). *Nucleon association in atomic nuclei and the nuclear reactions of the many nucleons transfers*. Kiev: Naukova dumka, 488.

Neudatchin, V. G., Kukulin, V. I., Boyarkina, A. N., and Korennoy, V. P. (1972). A microscopically substantiated optical potential for the α-t system, including nucleon exchange. *Lett. al Nuovo Cimento* 5, 834–838. doi:10.1007/BF02812319

Neudatchin, V. G., Kukulin, V. I., Korotkikh, V. L., and Korennoy, V. P. (1971). A microscopically substantiated local optical potential for α-α- scattering. *Phys. Lett. B* 34, 581–583. doi:10.1016/0370-2693(71)90142-0

Neudatchin, V. G., Kukulin, V. I., Pomerantsev, V. N., and Sakharuk, A. A. (1992). Generalized potential-model description of mutual scattering of the lightest *p+d, d+*^{3}He nuclei and the corresponding photonuclear reactions. *Phys. Rev. C* 45, 1512–1527. doi:10.1103/PhysRevC.45.1512

Neugart, R., Balabanski, D. L., Blaum, K., Borremans, D., Himpe, P., Kowalska, M., et al. (2008). Precision measurement of ^{11}Li moments: influence of halo neutrons on the ^{9}Li core. *Phys. Rev. Lett.* 101, 132502. doi:10.1103/PhysRevLett.101.132502

NIST (2019). Fundamental physical constants. Available at: https://physics.nist.gov/cuu/Constants/index.html (Accessed June 1, 2023).

Nollett, K. M., and Wiringa, R. B. (2011). Asymptotic normalization coefficients from *ab initio* calculations. *Phys. Rev. C* 83, 041001. doi:10.1103/PhysRevC.83.041001

Norman, E. B., and Schramm, D. N. (1979). On the conditions required for the *r*-process. *Astrophysical J.* 228, 881–892. doi:10.1086/156914

Nörtershäuser, W., Bushaw, B. A., Dax, A., Drake, G. W. F., Ewald, G., Götte, S., et al. (2005). Measurement of the nuclear charge radii of ^{8,9}Li. *Eur. Phys. J. A* 25, 199–200. doi:10.1140/epjad/i2005-06-053-9

Nuclear Data Evaluation Project (2021). Triangle universities nuclear laboratory. ^{8}Li β-decay evaluated data. Available at: https://nucldata.tunl.duke.edu/nucldata/GroundStatedecays/08Li.shtml#halflife (Accessed April 25, 2023).

Paradellis, T., Kossionides, S., Doukellis, G., Aslanoglou, X., Assimakopoulos, P., Pakou, A., et al. (1990). Astrophysical *S*(*E*) factor of ^{8}Li (α,n_0)^{11}B and inhomogeneous Big Bang nucleosynthesis. *Z. fur Phys. A At. Nucl.* 337, 211–220. doi:10.1007/BF01294294

Plattner, G. R., and Viollier, R. D. (1981). Coupling constants of commonly used nuclear probes. *Nucl. Phys. A* 365, 8–12. doi:10.1016/0375-9474(81)90384-5

Rauscher, T., Applegate, J. H., Cowan, J. J., Thielemann, F-K., and Wiescher, M. (1994). Production of heavy elements in inhomogeneous cosmologies. *Astrophys. J.* 429, 499. doi:10.1086/174339

Sánchez, R., Nörtershäuser, W., Dax, A., Ewald, G., Götte, S., Kirchner, R., et al. (2007). "Nuclear charge radius of ^{11}Li," in *Laser 2006* (Berlin, Heidelberg: Springer Berlin Heidelberg), 181–188. doi:10.1007/978-3-540-71113-1_17

Sargsyan, G. H., Launey, K. D., Shaffer, R. M., Marley, S. T., Dudeck, N., Mercenne, A., et al. (2022). Ab initio single-neutron spectroscopic overlaps in lithium isotopes. arXiv: 2210.08843 [nucl-th].

Su-Qing, H., Kai-Su, W., Yong-Shou, C., Neng-Chuan, S., and Zhi-Hong, L. (2010). The main path to C, N, O elements in big bang nucleosynthesis. *Chin. Phys. Lett.* 27, 082601. doi:10.1088/0256-307X/27/8/082601

Sukhoruchkin, S. I., and Soroko, Z. N. (2016). *Excited nuclear states*. Berlin Heidelberg: Springer. doi:10.1007/978-3-662-48875-1

Thielemann, F. K., Applegate, J. H., Cowan, J. H., and Wiescher, M. (1991). "Production of heavy elements in inhomogeneous cosmologies," in *Nuclei in the cosmos*. Editor H. Oberhummer (Baden/Vienna: Springer-Verlag, Heildelberg), 248.

Tilley, D. R., Cheves, C. M., Godwin, J. L., Hale, G. M., Hofmann, H. M., Kelley, J. H., et al. (2002). Energy levels of light nuclei *A*=5,6,7. *Nucl. Phys. A* 708, 3–163. doi:10.1016/S0375-9474(02)00597-3

Timofeyuk, N. K. (2013). Spectroscopic factors and asymptotic normalization coefficients for 0*p*-shell nuclei: recent updates. *Phys. Rev. C* 88, 044315. doi:10.1103/PhysRevC.88.044315

Varlamov, V., Ishkhanov, B., and Komarov, S. Y. (2015). *Nuclear wallet cards database*. Available at: http://cdfe.sinp.msu.ru/services/ground/NuclChart_release.html (Accessed June 1, 2023).

Wiringa, R. B. (2021). Spectroscopic overlaps. Available at: http://www.phy.anl.gov/theory/research/overlap (Accessed May 30, 2023).

Wuosmaa, A. H., Rehm, K. E., Greene, J. P., Henderson, D. J., Janssens, R. V. F., Jiang, C. L., et al. (2005). Neutron spectroscopic factors in ^{9}Li from ^{2}H(^{8}Li,p)^{9}Li. *Phys. Rev. Lett.* 94, 082502. doi:10.1103/PhysRevLett.94.082502

Zecher, P. D., Galonsky, A., Gaff, S. J., Kruse, J. J., Kunde, G., Tryggestad, E., et al. (1998). Measurement of the ^{8}Li(n,γ)^{9}Li cross section at astrophysical energies by reverse kinematics. *Phys. Rev. C* 57, 959–966. doi:10.1103/PhysRevC.57.959